

## Strongly dissipative processes in the $^{28}\text{Si} + ^{\text{nat}}\text{Si}$ reaction at 12.4 MeV/nucleon

P. Decowski,\* E. A. Bakkum, P. F. Box, K. A. Griffioen, R. Kamermans, and R. J. Meijer  
*Fysisch Laboratorium, Rijksuniversiteit Utrecht, 3508 TA Utrecht, The Netherlands*

(Received 12 November 1987)

The velocities of heavy residues with atomic numbers  $Z > 8$  were measured and analyzed in the  $^{28}\text{Si} + ^{\text{nat}}\text{Si}$  reaction at 12.4 MeV/nucleon. The average missing linear momentum transfer in the incomplete fusion processes for this symmetric system lies between 2.5% and 3.5%. The analysis revealed the existence of a fully damped component peaked strongly in the beam direction. The velocity distributions of this component seem to be determined mainly by recoils from secondary emitted particles.

### I. INTRODUCTION

In spite of rather abundant experimental data, the mechanisms of heavy-ion reactions at energies well above the Coulomb barrier are still far from being understood. Especially for light systems, where explicit quantal effects may play a bigger role than in the case of "semiclassical" heavy nuclei, it is difficult to construct a model of the observed phenomena. The mechanisms of fast particle emission, "incomplete fusion" or "cluster transfer,"<sup>1</sup> which accompany the fusion process, are still not well understood. At energies above 10 MeV/nucleon dissipative processes leading to projectile-like fragments with fully relaxed kinetic energies and evaporation-type angular distributions form a sizable part of the reaction cross section, but their origin (whether grazinglike<sup>2</sup> or fusionlike<sup>3</sup>) is still not clear. There are many theoretical approaches taken in explaining the complicated effects appearing in heavy-ion interactions, but none of them is fully successful. Time dependent Hartree-Fock (TDHF) calculations,<sup>4</sup> which only include the mean field aspects of the process, explain many of the general trends observed in the low energy experimental data. They also predict new effects such as transparency in interactions with small impact parameters, but in general fail to describe the data quantitatively. Recent semiclassical calculations based on the Landau-Vlasov approach,<sup>5</sup> which include individual nucleon-nucleon collisions in addition to mean-field effects, also are not able to provide a quantitative description of the experimental observations. Apparently there is a need for a more detailed and complete theory as well as more specific experimental data, which will help to establish the importance of various processes and to differentiate between the various models.

The results presented below are part of a systematic experimental investigation of fusion and fusionlike processes in rather light heavy-ion systems. A symmetric system like Si + Si provides the maximum compound-nuclear excitation energy per nucleon for a given bombarding energy. Moreover, the fore-aft symmetry of all observables in the center-of-mass frame simplifies the interpretation of the data.

A short description of the experimental details is given in Sec. II. Section III presents the procedure used in the

analysis of the data. The analysis was focused on the fusion and the most damped components seen in the velocity spectra. The results are discussed in Sec. IV.

### II. EXPERIMENT

Self-supporting  $^{\text{nat}}\text{Si}$  targets with a thickness of  $\sim 300 \mu\text{g}/\text{cm}^2$  were bombarded by  $^{28}\text{Si}^{9+}$  ions accelerated by the Kernfysisch Versneller Instituut (KVI) cyclotron to an energy of 347 MeV. The purity of the targets was tested before and after the experiment by scattering of 30 MeV  $^{12}\text{C}$  ions from the Utrecht tandem accelerator. During the experiment the amount of contaminants remained fairly constant,  $\sim 2\%$  of the target atoms were an admixture of heavy elements Fe, Cu, and Kr;  $\sim 4\%$  were atoms of C and  $\sim 4\%$  were atoms of O, the latter concentrated on the surfaces of the target.

The heavy residues of the reaction products were registered in the Utrecht time-of-flight (TOF)  $\Delta E$ - $E$  detection system<sup>6</sup> (see Fig. 1). The ionization chamber, backed by three large-area Si detectors (0.15, 0.5, and 0.15 mm thick, respectively) positioned  $1^\circ$  apart from each other with respect to the target, was mounted at the end of a 2 m long flight path. The time between the start signal from the microchannel plate detector and the stop signal from the Si detectors was measured with an accuracy of 700 ps. This resolution, which was limited by plasma delays in the Si counters and straggling in the gas, was sufficient to unambiguously distinguish the masses of all observed residues. This is shown in Fig. 2 which presents a plot of the quantity  $ET^2$  vs the energy  $E$  of the residues observed at  $5^\circ$ .

The off-line evaluation of the measured quantities provided energies, atomic numbers  $Z$ , mass numbers  $A$ , and velocities of residues with  $Z > 8$  (lighter elements were not fully stopped in the Si detectors). The time-of-flight information served only for the mass determination; the velocities were obtained from the measured energies and the evaluated masses of the residues. In this case the velocity spectra are not influenced by nonlinearities of time-to-amplitude converters and deceleration of ions in the ionization chamber. The data for all isotopes of a given element were summed to improve statistics and all results are presented as a function of  $Z$  values only.

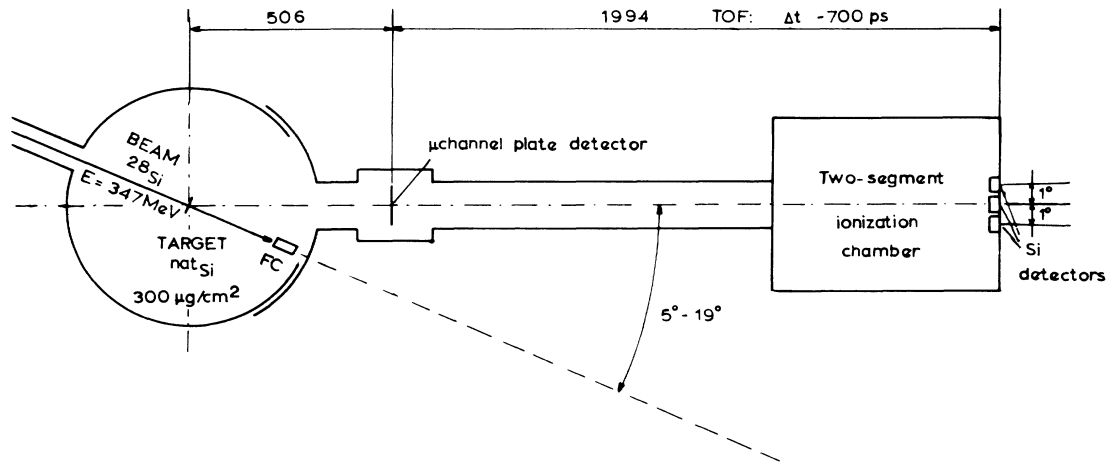


FIG. 1. Schematic diagram of the experimental setup.

The measurements were performed at angles between 5° and 19° in steps of 1°. The Faraday cup was only used for the relative normalization of the data. All cross sections given in the paper are expressed in terms of the fusion cross section, 570 mb, which is known from systematics.<sup>7</sup>

III. DATA ANALYSIS

Figure 3 shows examples of velocity spectra for Mg, P, and S nuclei observed at selected angles. Energy losses in the gas of the ionization chamber introduce low-velocity cutoffs in the spectra at about 1.5 cm/ns. Statistical calculations with the code PACE (Ref. 8) showed that a 4% admixture of oxygen in the target would give a maximal

contribution to the velocity spectra of elements with  $Z=15$  and  $16$  of  $\sim 9\%$  at  $6^\circ$  (residues from reaction on carbon peak at lower  $Z$  values and their contribution is relatively smaller because of the more abundant production of lighter elements in the reaction on silicon). The contribution of oxygen admixtures becomes negligible at  $9^\circ$ . For this reason the velocity spectra of the elements  $Z=15$  and  $16$  were analyzed only at angles larger than  $8^\circ$ .

The evolution of spectral shapes as a function of  $Z$  shows the high sensitivity of these velocity spectra to the different reaction mechanism. This feature is useful for identifying and extracting the various mechanisms in the reaction process. Velocities of residues with high  $Z$  values are centered at half of the beam velocity (2.4 cm/ns) in accordance with the expected fusion origin of these most heavy nuclei. Velocity spectra of nuclei with  $Z$  values close to that of the projectile exhibit a strong

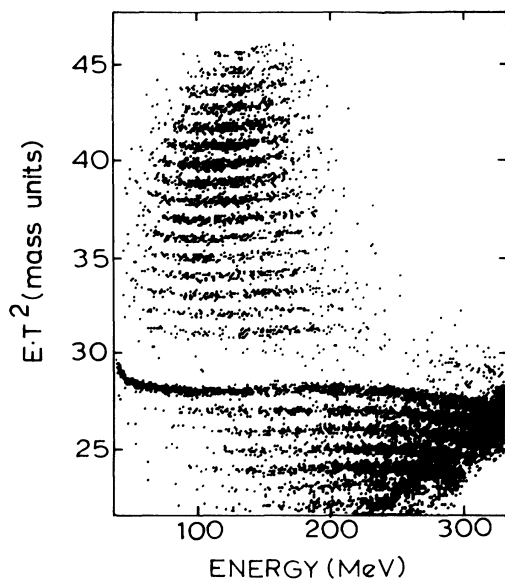


FIG. 2. Scatter plot of  $ET^2$  vs energy from off-line analysis of data registered at  $5^\circ$ . The events corresponding to  $Z$  value of the projectile (events contributing to mass numbers 27, 28, and 29) are scaled down by a factor of 100.

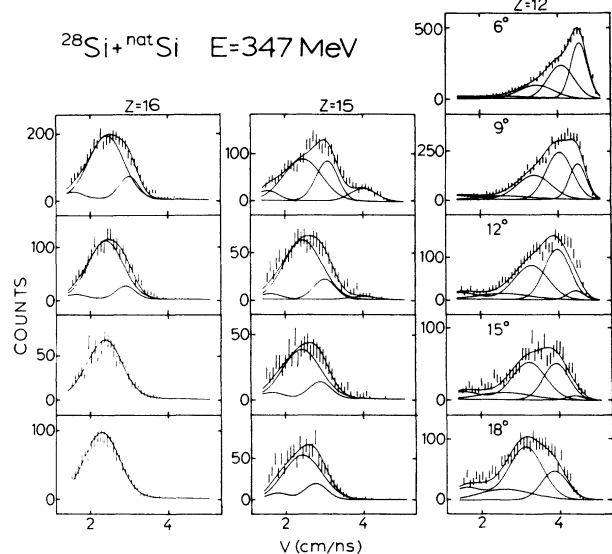


FIG. 3. Examples of the velocity spectra decomposition for selected angles and elements. The curves show the various components and the total fit.

component with beam velocity resulting from quasielastic processes. There is also an intermediate component clearly correlated with the  $Z$  value of the observed fragment.

With the help of a least-squares fitting routine all velocity spectra (240 in total) were decomposed according to the following procedure. The parameters of the Maxwellian shaped distributions connected with the fusion component (widths) can be determined from the data at large angles in the case of large  $Z$  values (see Fig. 3). The smooth  $Z$  dependence of the width (for given  $Z$  the width was assumed to be angle independent; it does not change more than a few percent in our angular range even if the invariant velocity distribution is quite anisotropic) can be extrapolated with the help of a polynomial fit into the region of smaller  $Z$  values, where a less intense fusion component is mixed with other processes. The same holds for the beam-velocity component, the parameters of which can be determined from the spectra at forward angles and  $Z < 14$ . Having determined those two most straightforward components, one can try to concentrate in detail on the region of intermediate velocities. The change of spectral shape with angle suggests the existence of two rather well-localized additional components with different degrees of damping. In the spectra of elements heavier than silicon the more damped component dominates the intermediate velocity region. For lighter elements an additional component at higher velocity appears at forward angles. It decreases at larger angles (see spectra for  $Z=12$  in Fig. 3) as well as with the growing difference between the fragment and projectile  $Z$  values. Both intermediate components were fitted with Maxwellian shaped distributions. Care was taken to ensure the consistency of the extracted parameters for all measured angles and  $Z$  values. Fits were done with the constraint of fore-aft symmetry in the center-of-mass frame (a velocity cut at  $\sim 1.5$  cm/ns as well as the reduced laboratory cross sections at low velocity hindered the independent analysis of the data in the region  $v < v_{c.m.}$ ).

#### IV. DISCUSSION

##### A. Fusion component

Figure 4 presents an example of the angular and velocity distributions of the half-beam velocity component for  $Z=19$  residues in the form of invariant cross section contours ( $d^3\sigma/d^3v$ ) in the  $(v_{\parallel}, v_{\perp})$  plane. The concentric lines follow the pattern typical for the random evaporation of particles from the compound nucleus, however, the width of the distribution along the beam direction is substantially larger than in the direction perpendicular to the beam (see Fig. 5, which shows the dependence of both widths on the residue  $Z$  value). The reason for this can be twofold. Large  $l$  components in the statistical decay of the compound nucleus will enhance the emission into forward and backward direction. Secondly, the incomplete fusion process introduces a spread of the initial compound nucleus velocity along the beam direction. To investigate in detail the contribution of the first process the response to the decay of the  $^{56}\text{Ni}$  compound nucleus was

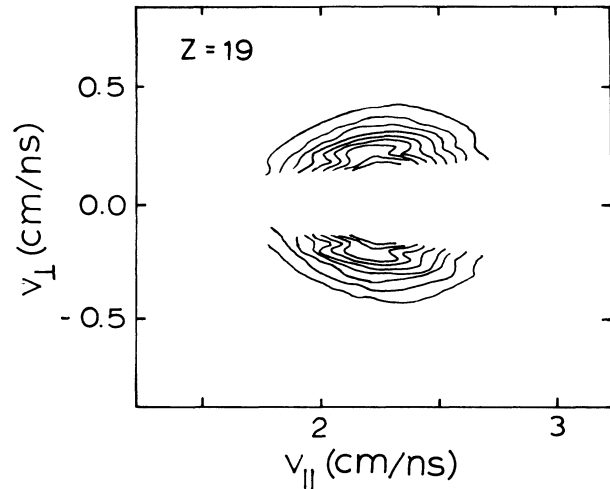


FIG. 4. Contour plot of the invariant cross section for the fusionlike component in the velocity spectra of the  $Z=19$  residue nuclei.

simulated by a Monte-Carlo PACE calculation,<sup>8</sup> using the value of  $l_{cr} = 44\hbar$  taken from systematics.<sup>7</sup> The calculated widths of the invariant cross sections in the directions parallel and perpendicular to the beam are presented in Fig. 5 as dashed and solid lines, respectively. In general, the calculated perpendicular widths agree quite well with the measured values (solid dots), except for the lowest  $Z$  values, for which the experimental distributions are broader. This may be attributed to the evaporation of heavier fragments ( $Z > 2$ ), which the PACE calculations did not take into account. Such a cluster emission makes it possible to evaporate more nucleons and thus should mainly influence the production of the lightest elements.

The center-of-mass angular distributions  $d\sigma/d\Omega_{c.m.}$  of the evaporation component may be parametrized using

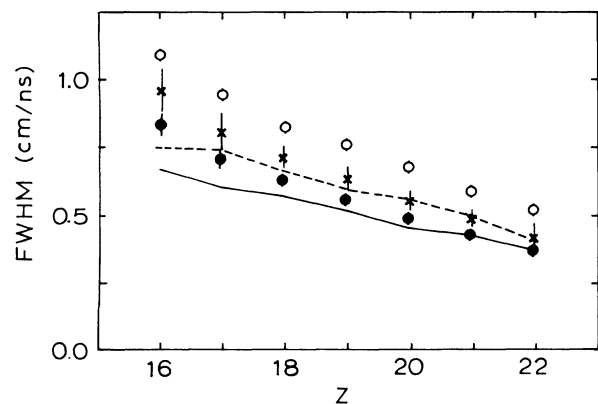


FIG. 5. Experimental widths of the fusionlike invariant velocity distributions in the direction parallel and perpendicular to the beam (open and full points, respectively). Dashed and solid lines present parallel and perpendicular widths given by statistical model PACE calculation. The crosses present the parallel width calculated from the experimental perpendicular width using the PACE value of the angular distribution coefficient  $k=0.45$ .

the form  $1/(\sin^2\theta_{c.m.} + k \cos^2\theta_{c.m.})^{1/2}$  ( $k=0$  corresponds to the classical  $1/\sin\theta_{c.m.}$  limit,  $k=1$  gives a distribution that is isotropic). Then the ratio of the velocity integrated Maxwellian-type distributions at  $0^\circ$  and  $90^\circ$  in the center-of-mass system is  $1/\sqrt{k}$ , which leads to the relation:

$$k = (W_{\perp}/W_{\parallel})^6, \quad (1)$$

where  $W_{\perp}$  and  $W_{\parallel}$  are the full widths at half maximum of the invariant cross section distribution in directions perpendicular and parallel to the beam.

Assuming that the admixture of heavy-fragment emission does not change substantially the average  $k$  value of the distributions, one can calculate from the experimental perpendicular widths the expected parallel widths,  $W_{\parallel}^{ev}$ , associated with the complete fusion (CF) compound nucleus decay using the average  $k$  value of  $0.45 \pm 0.13$  yielded by the PACE calculation (the  $k$  values from the PACE calculation are within the statistical error the same for all residues). The experimental parallel widths are much larger than the widths predicted by the statistical model (see Fig. 5). This should then be attributed to the contribution of the incomplete fusion (ICF) to the reaction process.<sup>9</sup>

In the center of mass of the symmetric system the invariant velocity distribution can be described by

$$F(v) = N_{CF} e^{-v^2/2\sigma^2} + N_{ICF} e^{-(v-\Delta v)^2/2(\sigma^2+\Sigma^2)} + N_{ICF} e^{-(v+\Delta v)^2/2(\sigma^2+\Sigma^2)}. \quad (2)$$

The last two terms stem from incomplete fusion processes, one caused by the projectile and the other by the target. Equation (2) contains two assumptions: (1) the incomplete fusion processes introduce a spread in the compound nucleus velocities which has a normal distribution with the average values  $\pm\Delta v$  and variance  $\Sigma^2$ ; (2) the variance of the evaporation residue distributions originating from incomplete fusion is the same as the variance  $\sigma^2 = (W_{\parallel}^{ev}/2.35)^2$  of residues from a fully fused system. In asymmetric systems the shift of the invariant velocity distribution centroid from a value expected for a completely fused system usually serves for determination of the average missing momentum transfer in the reaction.<sup>10</sup> This quantity represents the momentum deficit in the incomplete fusion process as well as the amount of the incomplete fusion. The experimental data indicate that the missing momentum is connected mainly with one, the lighter, partner of the reaction.<sup>11,12</sup> The symmetry of our system implies that an analysis based on the centroid of the measured distribution will yield an average missing momentum of zero. However, for comparison with systematics, one can deduce the same observables as extracted from the centroids in an asymmetric system by calculating the first moment of the distribution containing the incomplete fusion contribution only from one reaction partner:

$$F_1(v) = N_{CF} e^{-v^2/2\sigma^2} + N_{ICF} e^{-(v-\Delta v)^2/2(\sigma^2+\Sigma^2)}. \quad (3)$$

This calculation requires knowledge of three parameters:  $N_{ICF}/N_{CF}$ ,  $\Delta v$ , and  $\Sigma$ . The number of unknown param-

eters may be diminished with the help of the experimental observation that the shapes of the measured invariant distributions are well approximated by Gaussian curves. This means that the second and fourth moments of the distribution  $F(v)$  [Eq. (2)] are connected by the Gaussian relation:

$$M_4 = 3M_2^2. \quad (4)$$

Another constraint follows from the demand that the second moment of the distribution  $F(v)$  is equal to the variance of the experimental distribution  $(W_{\parallel}^{exp}/2.35)^2$ . Finally, we are then left with one unknown parameter. If we choose it in the form  $\gamma = (\Sigma/\Delta v)^2$  we can express the other two parameters in the form:

$$\Delta v = (W_{\parallel}^{ev} \delta / 2.35) [3(\gamma + 1) / (6\gamma + 3\gamma^2 + 1)]^{1/2},$$

$$N_{ICF} / N_{CF} = [ (6\gamma + 3\gamma^2 + 1)^3 / (6\gamma + 3\gamma^2 + 1 + 3\gamma(\gamma + 1)\delta^2) ]^{1/2} / 4,$$

where

$$\delta = (W_{\parallel}^{exp2} - W_{\parallel}^{ev2})^{1/2} / W_{\parallel}^{ev}. \quad (5)$$

The average missing momentum determined by the first moment of the distribution  $F_1(v)$  [Eq. (3)] can be calculated from the formula:

$$\left\langle \frac{\Delta p}{p} \right\rangle = (W_{\parallel}^{ev} \delta / v_{c.m.} / 2.35) \times [3(\gamma + 1)(6\gamma + 3\gamma^2 + 1)]^{1/2} / (6\gamma + 3\gamma^2 + 5). \quad (6)$$

Figure 6 shows the  $\gamma$  dependence of  $\Delta p/p$ ,  $\Delta v$  and the relative amount of the incomplete fusion, averaged over  $Z$  values between 16 and 22 (the ratio of  $\Delta p/p$  for  $Z=16$  and 22 is  $\sim 1.8$ ). In the limit of  $\Sigma=0$  ( $\gamma=0$ ), which is equivalent to the assumption of the spectator-participant breakup-fusion picture with one incomplete fusion channel dominating, one obtains  $\Delta p/p \approx 2.5\%$ , an ICF/(ICF + CF) ratio of  $\approx 20\%$  and  $\Delta v$  reaches the maximum value of 0.3 cm/ns. In this simplified picture such velocity shift corresponds to the emission, on the average, of  $\sim 6$  nucleons with beam velocity. When  $\gamma$  increases,  $\Delta p/p$  approaches a maximum of 4% at  $\gamma \approx 1$  and tends to zero as  $\gamma$  goes to infinity. However, the value of  $\gamma \approx 1$  corresponds to ICF/(ICF + CF)  $\approx 70\%$ , whereas the contribution of the incomplete fusion in the asymmetric system  $^{20}\text{Ne} + ^{27}\text{Al}$  at the same relative velocity at the top of the Coulomb barrier (4.4 cm/ns), deduced from the shape of the invariant velocity distribution, is only  $\sim 30\%$  (Ref. 10). We think that an upper limit of  $\sim 50\%$  of incomplete fusion contribution in our reaction is thus a quite conservative assumption. With this assumption we obtain a value of the average missing momentum which lies between 2.5 and 3.5%. These numbers should be compared with the value averaged over all residues of 7% obtained from systematics for asymmetric systems like  $^{20}\text{Ne} + ^{27}\text{Al}$  at the same relative velocity at the moment of contact.<sup>10</sup> Smaller values of the average missing momentum transfer seem to reflect the general trend

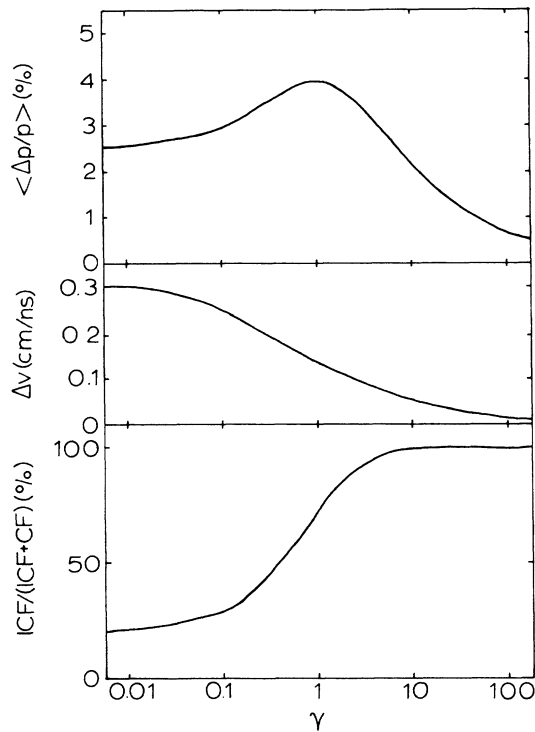


FIG. 6. The dependence of the average missing momentum transfer, velocity shift, and the amount of the incomplete fusion on the parameter  $\gamma$  (see text).

which shows for symmetric systems a reduction of the effects that lead to the incomplete fusion.<sup>12-15</sup> In principle this is what one would expect if the missing momentum is directly connected to the sudden deceleration of the particle during contact with the partner. In the case of  $^{28}\text{Si} + ^{28}\text{Si}$  at our energy the change of the bombarding particle velocity (as well as the target nucleus velocity) during the nuclear interaction is  $\sim 2.2$  cm/ns (the gentle deceleration caused by the Coulomb field taken into account). For asymmetric systems the lighter partner feels the highest deceleration. In the  $^{20}\text{Ne} + ^{27}\text{Al}$  reaction an initial energy of  $\sim 10$  MeV/nucleon is needed to produce Ne ions with the velocity of 2.2 cm/ns at the top of the Coulomb barrier. The average missing momentum at the energy of 10 MeV/nucleon is  $\sim 4\%$  (Ref. 10), which is much closer to the value observed in our system.

The angular distributions of the fusionlike component are shown in Fig. 7(a). Their shapes can be described by Gaussian functions [solid lines in Fig. 7(a)]. The integrated cross sections are presented in Fig. 7(b) as open bars. A PACE calculation (solid bars in Fig. 7) describes the shape of the element distribution for higher  $Z$  values but underestimates the cross section for the lighter residues. Again this could be a signature of the sizable contribution of the emission of heavier fragments in the compound nucleus decay. Similar effect could be caused by the incomplete fusion processes producing lighter and less excited compound nuclei. However, the small value of the extracted average missing linear momentum rules out this possibility.

## B. Dissipative component

Figure 8 shows contours representing invariant cross sections in the  $Z$  vs  $v$  plane which are connected with the more dissipative intermediate component extracted from the velocity spectra at  $6^\circ$ . The centroids of the distributions are directly related to the Coulomb repulsion velocities in the center-of-mass frame assuming a binary process (solid line in Fig. 8). This is a signature of the full relaxation of the kinetic energy. The angular distributions in the center-of-mass system evaluated with the assumption of a binary process are peaked forward. For the lightest elements the distribution falls off slower than  $1/\sin\theta_{\text{c.m.}}$  dependence expected in the fusion-fission process; for the largest  $Z$  values the opposite is true. However, if one plots the invariant cross section contours in the  $v_{\parallel}$  vs  $v_{\perp}$  plane, a striking correlation between the angular and velocity distributions shows up (Fig. 9). The contours are fairly circular. The circular shapes of the constant cross section lines suggest that at forward angles the spread in velocity and angle is mainly determined by secondary particle emission from slowed-down fragments. The source velocities must then be strongly forward peaked. The observed local maxima and plateaus coincide with the recoil velocities corresponding to the emission from the excited fragments of the complex par-

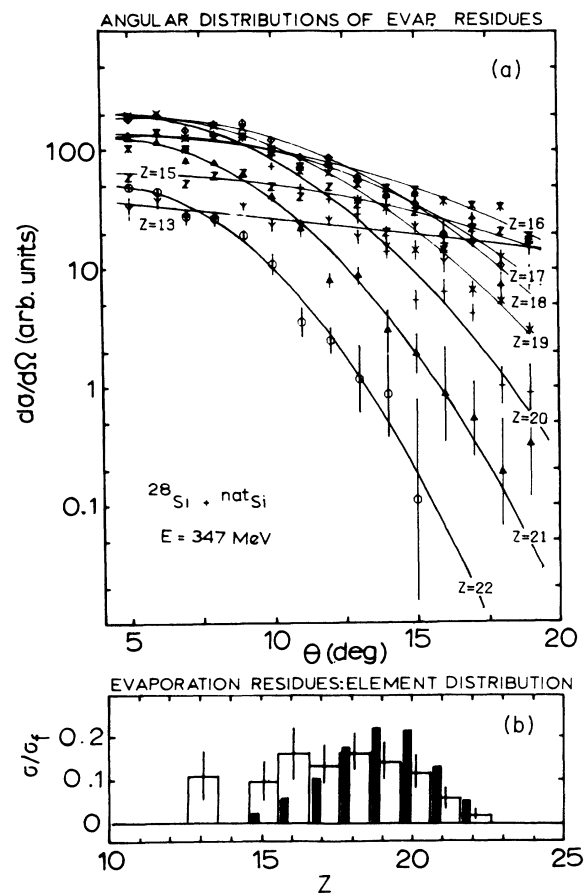


FIG. 7. (a) Angular distributions and (b) element distribution of compound-nucleus residues (open bars). The solid bars show the results of statistical model calculation with  $l_{cr} = 44\hbar$ .

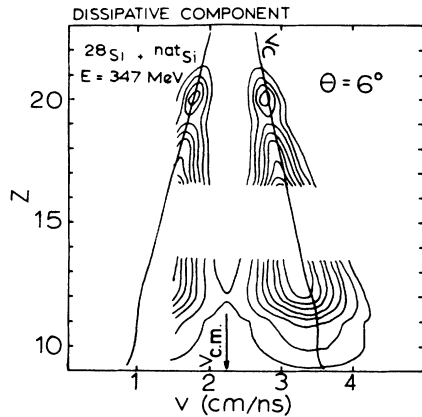


FIG. 8. Contour plots of the dissipative component at  $6^\circ$  in the  $Z$  vs  $v$  plane. The symbols  $v_{c.m.}$  and  $v_c$  describe the center-of-mass velocity and the velocity in the center-of-mass frame corresponding to the fragment Coulomb energy (see text), respectively. The solid thick lines describe the dependence of the Coulomb velocity on the  $Z$  value of the fragment.

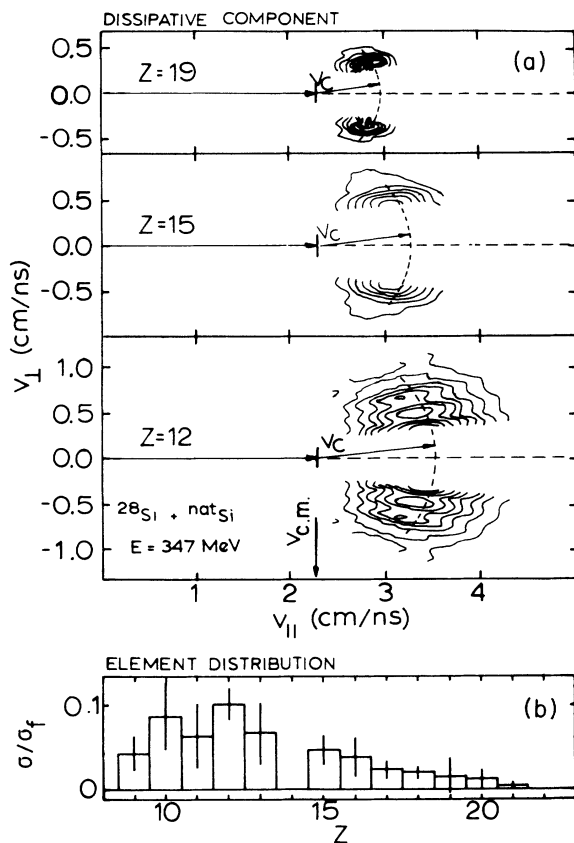


FIG. 9. Contour plots of invariant cross section for the dissipative component in the velocity spectra of elements Mg, P, and K (a) and the element distribution of the dissipative component (b). The contour plots are presented for  $v$  transverse ( $v_\perp$ ) vs  $v$  parallel ( $v_\parallel$ ) to the beam. The symbols  $v_{c.m.}$  and  $v_c$  describe the center-of-mass velocity and the velocity in the center-of-mass frame corresponding to the fragment Coulomb energy (see text), respectively.

ticles  $^8\text{Be}$  and  $^{12}\text{C}$  with energies close to the Coulomb barrier.

Thus the strongly forward-peaked component shows the combination of very little relaxation of transverse degrees of freedom and full kinetic energy relaxation, i.e., a full relaxation of the degrees of freedom parallel to the beam. The total cross section of this strongly damped process equals to half of the fusion cross section. Also, the element distribution of the integrated cross section [Fig. 9(b)], peaking at  $Z$  slightly smaller than  $Z$  of the projectile, shows that on the average the nuclear matter flow during the interaction is small. Such a dissipative component at very forward angles is not reproduced in diffusion model<sup>16</sup> calculations (although questionable for such light nuclei), which for Si + Si predict a strong correlation between scattering angle and energy relaxation and yield full kinetic-energy damping only in the orbiting limit. In principle the observed features—strong forward focusing and full kinetic energy relaxation—are typical effects which can be expected from a low  $l$  transparency window observed in a mean field approach by TDHF calculations.<sup>4</sup> One expects that the individual nucleon-nucleon collisions will decrease this transparency. Indeed, recent Landau-Vlasov calculations show that for the  $^{28}\text{Si} + ^{28}\text{Si}$  system at 12.4 MeV/nucleon the influence of collisions is strong enough to destroy the transparency.<sup>17</sup> However, there are grounds to think that the number of collisions in this type of calculations is overestimated.<sup>18</sup> Another possible interpretation of the observed component could be the superposition of near-side and far-side grazing trajectories in the deep inelastic collision, which could lead to strong focusing in the forward direction. In this way, a strongly forward-peaked component observed in the asymmetric system  $^{16}\text{O} + ^{48}\text{Ti}$  at the lower energy of 6.3 MeV/nucleon (Ref. 19) was successfully explained. Such effect appears when the width of the grazing angle distribution is much larger than the average grazing angle. However, it is difficult to understand in our case how such effect could lead to the observed typical correlation, for each  $Z$  value, between the widths in the perpendicular and parallel directions of invariant cross section.

## V. CONCLUSIONS

In summary, the fusion and dissipative components in the  $^{28}\text{Si} + ^{\text{nat}}\text{Si}$  system were studied at forward angles and could be extracted from the velocity spectra. The widths of the fusionlike component distribution show the contribution of the incomplete fusion for this symmetric system, yielding an average missing linear momentum transfer between 2.5 and 3.5%. At forward angles, a dissipative component, characterized by full damping of the kinetic energy, exhibits strong forward peaking with little relaxation in the angular degrees of freedom. Full relaxation of the kinetic energy is typical for a deep inelastic product; however, the expected relation between kinetic-energy loss and scattering angle for deep inelastic collisions was not observed. The dissipative component is hard to understand in the framework of the conventional picture of damped heavy-ion interactions.<sup>20</sup>

## ACKNOWLEDGMENTS

We would like to thank the staff of KVI (Groningen) for supplying us with the heavy ion beam. This work was

performed as a part of the research program of the "Stichting voor Fundamenteel Onderzoek der Materie" with financial support from the Nederlandse Organisatie voor Zuiver-Wetenschappelijk Onderzoek.

\*On leave from the Institute of Experimental Physics, University of Warsaw, Warsaw, Poland.

<sup>1</sup>H. Morgenstern, W. Bohne, W. Galster, and K. Grabisch, *Z. Phys. A* **324**, 443 (1986).

<sup>2</sup>D. Shapira, D. DiGregorio, J. Gomez del Campo, R. A. Dayras, J. L. C. Ford, Jr., A. H. Snell, P. H. Stelson, R. G. Stokstad, and F. Pougheon, *Phys. Rev. C* **28**, 1148 (1983).

<sup>3</sup>R. J. Charity, M. A. McMahan, D. R. Bowman, Z. H. Liu, R. J. McDonald, G. J. Wozniak, L. G. Moretto, S. Bradley, W. L. Kehoe, A. L. Mignerey, and M. N. Namboodiri, *Phys. Rev. Lett.* **56**, 1354 (1986).

<sup>4</sup>K. T. R. Davies, K. R. S. Devi, S. E. Koonin, M. R. Strayer, in *Treatise on Heavy-Ion Science*, edited by D. A. Bromley (Plenum Press, New York, 1984), Vol. 3.

<sup>5</sup>C. Gregoire, B. Remaud, F. Seville, L. Vinet, and Y. Raffray, *Nucl. Phys. A* **465**, 317 (1987). H. Kruse, B. V. Jacak, J. J. Molitoris, G. D. Westfall, and H. Stocker, *Phys. Rev. C* **31**, 1770 (1985). J. Aichelin and H. Stocker, *Phys. Lett.* **163B**, 59 (1985).

<sup>6</sup>E. A. Bakkum, A. van den Brink, R. J. Meijer, and R. Kamermans, *Nucl. Instrum. Methods A* **243**, 435 (1986).

<sup>7</sup>W. W. Wilcke, J. R. Birkelund, H. J. Wollersheim, A. D. Hoover, J. R. Huizenga, W. U. Schroder, and L. E. Tubbs, *At. Data Nucl. Data Tables* **25**, 389 (1980).

<sup>8</sup>A. Gavron, *Phys. Rev. C* **21**, 230 (1980).

<sup>9</sup>H. J. Keim, B. Kohlmeyer, H. Stege, H. A. Boesser, F. Puehlhofer, and W. F. W. Schneider, *Z. Phys. A* **327**, 1010 (1987).

<sup>10</sup>H. Morgenstern, W. Bohne, K. Grabisch, H. Lehr, and W.

Stoeffler, *Z. Phys. A* **313**, 39 (1983).

<sup>11</sup>Y. Chan, M. Murphy, R. G. Stokstad, I. Tserruya, S. Wald, and A. Budzanowski, *Phys. Rev. C* **27**, 447 (1983).

<sup>12</sup>H. Morgenstern, W. Bohne, W. Galster, K. Grabisch, and K. Kyanowski, *Phys. Rev. Lett.* **52**, 1104 (1984).

<sup>13</sup>S. E. Vigdor, D. G. Kovar, P. Sperr, J. Mahoney, A. Menchaca-Rocha, C. Olmer, and M. S. Zisman, *Phys. Rev. C* **20**, 2147 (1979).

<sup>14</sup>G. Rosner, J. Pochodzalla, B. Heck, G. Hlawatsch, A. Miczajka, H. J. Rabe, R. Butsch, B. Kolb, and B. Sedelmeyer, *Phys. Lett.* **150B**, 87 (1985).

<sup>15</sup>J. D. Hinnefeld, Ph.D. thesis, University of Notre Dame, 1987; J. D. Hinnefeld, J. J. Kolata, D. J. Henderson, R. V. F. Janssens, D. G. Kovar, K. T. Lesko, G. Rosner, G. S. F. Stephans, A. M. van den Berg, B. D. Wilkins, F. W. Prosser, S. V. Reinert, and P. L. Gonthier, *Phys. Rev. C* **36**, 989 (1987).

<sup>16</sup>H. Feldmeier, *Nukleonika* **25**, 171 (1980); H. Feldmeier and H. Spangerberger, *Nucl. Phys. A* **248**, 223c (1984).

<sup>17</sup>C. Gregoire, B. Remaud, F. Seville, L. Vinet, and D. Jacquet, Proceedings of the International Workshop on Semi-classical and Phase-space Approaches to the Dynamics of the Nucleus, Aussois, 1987 [*J. Phys. C* **2**, **203** (1987)].

<sup>18</sup>W. Bauer, G. F. Bertsch, and S. Das Gupta, *Phys. Rev. Lett.* **58**, 863 (1987).

<sup>19</sup>R. Ritzka, W. Dünneweber, A. Glaesner, W. Hering, H. Puchita, and W. Trautmann, *Phys. Rev. C* **31**, 133 (1985).

<sup>20</sup>P. Decowski, E. A. Bakkum, P. Box, K. A. Griffioen, R. Kamermans, and R. J. Meijer, *Z. Phys. A* **327**, 235 (1987).